BER the international journal of bridge engineering management and research

Examples of Bridges Designed with Pultruded GFRP Trusses

Giuseppe Campione*

Submitted: 14 August 2025 **Accepted:** 15 September 2025 **Publication date:** 10 January 2026

DOI: 10.70465/ber.v3i1.70

Abstract: The specific application of glass fiber reinforced polymer (GFRP) truss structures could replace the concrete deck and prestressed beams damaged by corrosion processes in single-span bridges while maintaining the piers and the foundation. This solution produces a significant reduction in seismic mass, with a consequent reduction of the lateral forces on piers and foundation, and potentially cheaper strengthening of piers and foundation for seismic purposes. The novelty of the research also lies in the application of recent pre-code documents for the design of GFRP bridges, which are not explicitly mentioned in the abovementioned pre-code documents. Also, a proposal is made for limits on cross-section maximum slenderness and element slenderness, with suggestions for the best joints to connect single elements.

Author keywords: GFRP road bridge; Local buckling; Global buckling; Long-term effects; Shear deformation

Introduction

The need for a lightweight and highly durable structure, especially in particularly aggressive environments such as the marine ones, has led bridge designers to consider the use of pultruded glass fiber reinforced polymer (GFRP) material. This material is produced with continuous glass fibers and resin through an industrial process to obtain one-dimensional elements with geometric shapes very similar to those of traditional carpentry, characterized by a much lower specific weight than that of steel and less susceptibility to atmospheric and corrosive agents. The significant reduction in fixed loads on the foundation abutments compared to the use of a metal carpentry structures, and above all the handling and installation of the structure using low-capacity lifting machines, and, consequently, small dimensions with extremely limited operating spaces on the construction site, show the indisputable advantages of using pultruded materials for constructing composite bridges. Alongside these indisputable advantages, there are several disadvantages, such as sensitivity to viscous effects; the dynamic behavior of a structure with low self-weight and low elastic modulus, making it susceptible to vibrations induced by traffic and pedestrians; fragile behavior at failure; and second-order effects that affect its design.

Today there are many examples of pedestrian bridges designed with variable loads between 3 and 5 kN/m^2 and built with structures formed by full-wall or lattice beams with spans between 10 and 20 m and a height of a couple of meters. In contrast, there are few constructions for road bridges, where much higher variable loads between 15 and 30 kN/m^2 and maximum deflection values between 1/300 and 1/600 of the span lead to heavy sizing that justify their construction only in particular conditions where the use of steel is not recommended. Fig. 1 shows an example of a pedestrian bridge built with lattice beams made from pultruded GFRP elements. The bridge is in Rotterdam and it is of the maritime type. The truss is formed with elements having double T sections assembled with bolted joints. It should be noted that most FRP pultruded bridges are pedestrian bridges, while in the field of road bridges, among the few achievements, we can mention the Marshal Jozef Pilsudski bridge in Poland, whose width has been expanded in the lateral cycle walkways from 2 to 4.5 m with triple cavity pultruded profiles with a 500 × 150 mm section, and the bridge in Rotterdam in Holland, where the deck is made of a pultruded GFRP grating (see Fig. 2).

Figure 1. Example of GFRP pedestrian bridge.
GFRP, glass fiber reinforced polymer

In the United States, a pultruded GFRP bridge has been designed and built that supports 4.5-ton vehicles. The bridge is eco-sustainable, resistant to corrosion, and boasts the lowest cost of ownership for its entire life cycle.

*Corresponding Author: Giuseppe Campione.
Email: studioingcampione@libero.it
Ph.D, Full Professor of Structural Engineering at Department of Engineering, University of Palermo, Viale delle Scienze, 90128 Palermo, Italy

Discussion period open till six months from the publication date. Please submit separate discussion for each individual paper. This paper is a part of the Vol. 3 of the International Journal of Bridge Engineering, Management and Research (© BER), ISSN 3065-0569.

Figure 2. Road bridge in Rotterdam in GFRP.
GFRP, glass fiber reinforced polymer

Several past studies on truss bridge behavior are available in the literature.[1–7] However, even today, the use of pultruded GFRP for structural elements in infrastructures and bridges is limited, also because very few documents and pre-codes[8–10] provide details for their design at the ultimate and serviceability limit states, and none of them refer explicitly to bridge truss structures.

A structural typology that is very suitable for the construction of bridges is the truss structure, which, however, as observed in many experimental researches available in the literature[11,5–7] is very sensitive to compressive stresses with local and global buckling and, above all, shows vulnerability in bolted and glued connections.

CNR-DT 205,[8] ASCE/SEI 74,[10] and other pre-code documents provide details for the design of GFRP structures and the calculation of bolted and adhesive joints for connecting pultruded FRP elements. In this paper, a design methodology is proposed for medium-span road bridges and pedestrian bridges with a spatial truss beam structure, focusing on the choice of profile shapes, types of truss beams, and connection types, while stressing the main differences in the design of pedestrian and road GFRP bridges. This research aims to propose the use of GFRP truss structures to replace concrete decks and prestressed beams damaged by corrosion processes in single-span bridges while maintaining the piers and the foundation. The proposal utilizes the recent pre-code LRFD[10] and CNR-DT 207[8] to investigate the use of GFRP elements for the design of road and pedestrian bridges, with the limitations due to long-term effects, strength and deflection characteristics, and also connection design aspects.

Truss Shapes for Pultruded GFRP Bridges

Trusses are structural frames formed by one or more triangles with elements in compression or in tension connected at the joints, assumed to be frictionless hinges or pins that allow the ends of the members to rotate slightly, thus creating a stable shape or configuration.

In this section, an example of a road bridge (see Fig. 3) is presented, made of plane or spatial trusses of height h placed longitudinally with span L and transversally with depth B.

The design load for road bridges at the operating limit state was estimated at 900 daN/m^2, with a concentrated load of 30 kN at the middle of the beam. For pedestrian bridges, a design load of 400 daN/m^2 was considered, with no concentrated load.

The deck is made of pultruded GFRP (see e.g., Li et al.[12]), with height h_1, with top and bottom flanges of thickness t_1, and webs placed at pitch s with thickness t_2.

Fig. 4 shows a drawing of a deck in GFRP also with GFRP H beams (see e.g., Li et al.[12]).

The joints between the truss elements are made as shown in Fig. 5 with steel plates connected by bolts.[11,13] GFRP elements are glued to stainless steel tubes placed inside the GFRP profile with a gluing length of 120 mm. The steel tubes are welded to steel plates and these are connected to the joints by high-strength bolts.

Table 1 gives some indicative ranges of mechanical characteristics of pultruded GFRP elements.

Referring to the single plane or spatial trusses with the collaboration of the GFRP deck of inertia J_d and area A_d, it is possible to derive the inertia and the modulus of strength of equivalent solid beams having the same inertia and strength modulus as the trusses. The geometrical properties of the equivalent beams can be found in Table 2. Cases of one or two upper elements or two lower elements are considered (cases a, b, c in Table 2).

For the preliminary design of a truss, we refer to the static scheme of a simply supported beam of length L at the ends, loaded with uniform loads q_{sle} and q_{slu} and a concentrated load P (in the case of a road bridge).

The strength and deformability checks are based on the use of the following expressions, which give the required strength modulus and inertia for a given design strength and deflection limit δ_0:

$$W_e = \left(\frac{1}{2}\cdot q_{SLU}\cdot L + P_{SLU}\right)\cdot\frac{L}{4\cdot f_{yd}} \tag{1}$$

$$\delta = \frac{L^3}{8\cdot E_1\cdot J}\left(5\cdot q_{SLE}\cdot L + P_{SLE}\right) + \frac{L}{4\cdot k\cdot G\cdot A}$$
$$\left(\frac{1}{2}\cdot q_{SLE}\cdot L + P_{SLE}\right) \le \delta_0\ k = \frac{20\cdot(1+\upsilon)}{48+39\cdot\upsilon} \tag{2}$$

For the deformability check, the elastic module E_1 was reduced by 0.66 and G by 0.448 to account for viscosity, as suggested by CNR-DT 207[8] (assuming a useful life of 10 years as temporary structures), while the strength was reduced by the product of 1.35 × 1.15, as suggested in CNR-DT 207.[8]

Strength Verification of Strut and Tie Elements of Trusses

In this section, some expressions available in the literature for the strength verification of truss elements are presented, taking into account the local and global buckling of pultruded members.

CNR-DT 207[8] and ASCE/SEI 74[10] were utilized for the design of elements and connections using GFRP profiles.

The connection between the single elements in the joints is assumed to be made with steel bolted plates (see

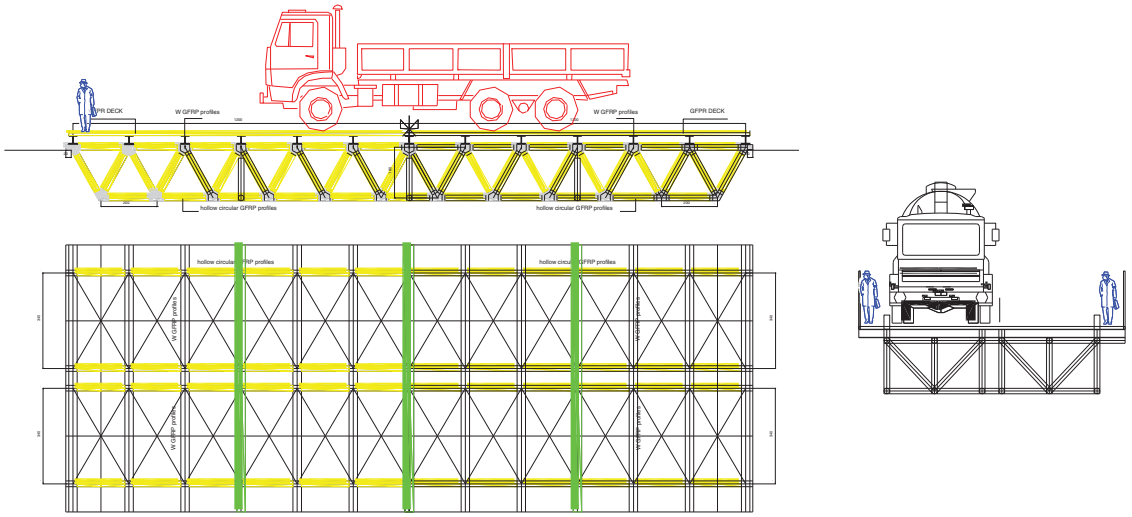

Figure 3. Proposal of pultruded GFRP bridges. GFRP, glass fiber reinforced polymer

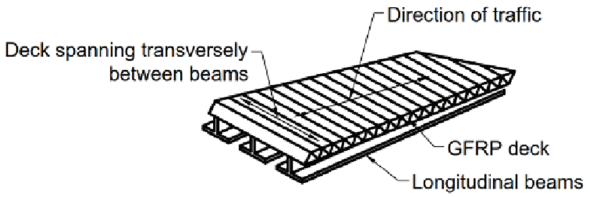

Figure 4. Proposal of GFRP deck. GFRP, glass fiber reinforced polymer

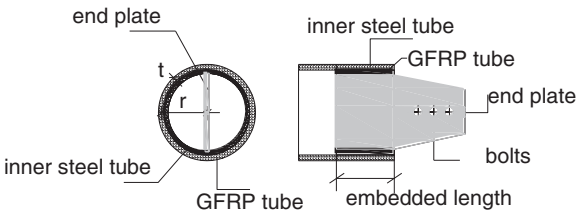

Figure 5. Proposal of joint connection for circular cross-sections. GFRP, glass fiber reinforced polymer

e.g., Hao et al.[13]), while the connection between the plates and GFRP elements is assumed to be glued (see e.g., Higgoda
et al.[7]).

Elements in tension are verified referring to the gross area of the cross-section purged of the area of the bolts (if any) and to the tensile design strength of the material. The tensile strength of the material is obtained through direct tensile tests on coupons, while compression tests are performed on stub elements.

CNR-DT 207[8] adopts a safety factor for the material depending on the uncertainties related to the determination of the material properties for a given coefficient of variation and an additional coefficient that accounts for the brittle behavior of the composite, leading to an overall coefficient that in the most severe case is 1.495. This coefficient, utilized to reduce the strength, is equal to 0.668, which is close to the coefficient of 0.7 assumed by ASCE/SEI 74.[10]

CNR-DT 207[8] takes into account the viscoelastic effects of the composite, penalizing the elastic module with coefficients equal to 0.3 and 0.5 for quasi-permanent loads and fatigue, respectively.

In compression, in the absence of experimental values, it is possible to predict analytically the compressive strength, as done by Cardoso et al.,[14] with a simple expression:

$$\sigma_m = G \cdot (1 + \chi_{cr}/a)^b \tag{3}$$

where a, b, and χ_{cr} are the coefficients that are assumed in Eq. (1) as 0.21, −0.69, and 5.148, respectively, as suggested by Cardoso et al.,[14] which give:

$$\sigma_m = 0.107 \cdot G \tag{4}$$

In this paper, the longitudinal elastic modulus of GFRP has been related to the compressive strength with a linear relationship of the following form:

$$E_1 = 100 \cdot \sigma_m \quad \text{(MPa)} \tag{5}$$

By adopting Eqs. (4) and (5), it is possible to construct the diagram of Fig. 6, which provides the variation of the longitudinal and tangential elastic modulus (Eq. (3)) with the compressive strength. In the same graph, some experimental data available in the literature are reported (data of Pecce and Cosenza[15]).

It can be seen that the correlation proposed by Cardoso et al.[14] gives an excellent interpolation of the experimental data when $G = 1/9\ E_1$. Eq. (5) is safe with respect to the available experimental data and has the advantage over Eq. (4) that its use is related to the determination of E_1, which is easier to determine experimentally than G.

Table 3 gives expressions for critical stress for hollow square and circular cross-sections. CNR-DT 207[8] does not give any analytical expression for the calculation of critical stress of circular cross-sections.

Most of these expressions for hollow circular cross-sections are derived from equations originally proposed by

Table 1. Indicative mechanical properties for GFRP elements

Density	γ (daN/m^3)	1600–2100
Tensile strength (coupons)	σ_t (MPa)	200–500
Elastic modulus in tension (coupons)	$3E_1$ (GPa)	20–30
Shear modulus (profile)	G (GPa)	3–5
Longitudinal Poisson coefficient	v_{12}	0.23
Transversal Poisson coefficient	v_{21}	0.09

GFRP = glass fiber reinforced polymer.

Table 2. Properties of transverse section of truss

Properties	a)	b)	c)
	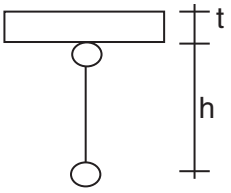	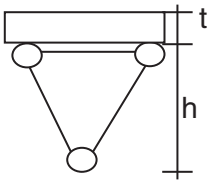	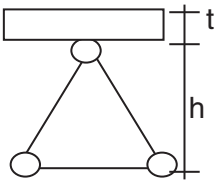
Without deck			
At	2 A	3 A	3 A
J	0.5 Ah^2	2/3 Ah^2	1 Ah^2
With deck			
yG	$\frac{A_d + A}{2 \cdot A + A_d} \cdot h$	$\frac{A_d + 2 \cdot A}{3 \cdot A + A_d} \cdot h$	$\frac{A_d + A}{3 \cdot A + A_d} \cdot h$
J	$J_D + A_d \cdot \left(\frac{h}{2}\right)^2 + + A \cdot (h - y_G)^2 + A \cdot {y_G}^2$	$J_D + A_d \cdot \left(\frac{h}{2}\right)^2 + + 2 \cdot A \cdot (h - y_G)^2 + A \cdot {y_G}^2$	$J_D + A_d \cdot \left(\frac{h}{2}\right)^2 + + A \cdot (h - y_G)^2 + 2 \cdot A \cdot {y_G}^2$

At = whole gross area of currents; h = distance between currents.

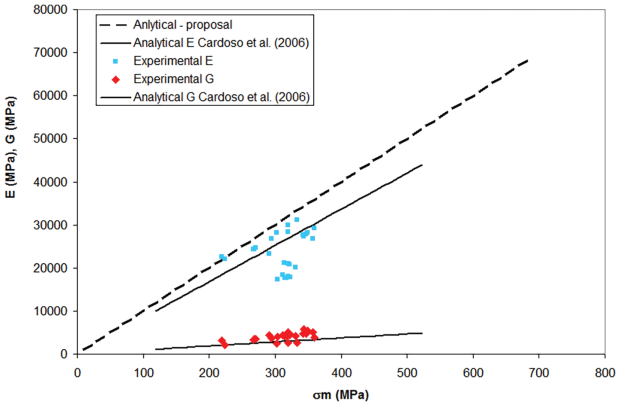

Figure 6. Variation of longitudinal and shear modulus with compressive strength

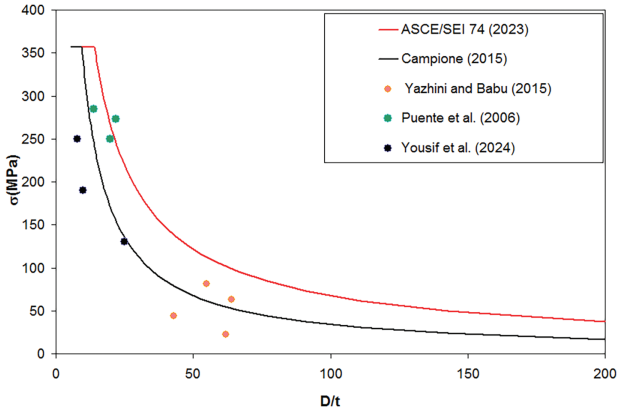

Figure 7. Variation of critical stress with D/t

Timoshenko and Gere[16] for homogeneous isotropic materials and corrected to account for the anisotropy of the material through the introduction of the longitudinal and transversal module of elasticity (E_1, E_2) and the Poisson coefficients v_{12} and v_{21}. Adopting the equation given by ASCE/SEI 74[10] with E2 = 1/3 E 1 and setting it equal to Eq. (5) gives the maximum D/t value of 54 to avoid strength reduction in compression due to buckling effects.

Fig. 8 shows a comparison between the critical stress determined with ASCE/SEI 74[10] and the proposed model with variation in D/t. The comparison is made for material with E_1 = 23 GPa, E_2/E_1 = 1/3, G/E_1 = 1/9 (with $E_1 > E_2$).

Table 3. Expressions for critical stress available in the literature

Cross-section	References	Expression of critical stress σ_{cr}
Hollow square	MMFG (1990)	$\frac{E_1}{2 \cdot (2 \cdot b/t)^{1.5}}$
Hollow square	Srongwell[17]	$\frac{E_1}{16} \cdot \left(\frac{t}{b}\right)^{0.85}$
Hollow circular	ASCE/SEI 74[10]	$\frac{2 \cdot t}{D} \cdot \min\left(\sqrt{\frac{E_1 \cdot E_2}{3}}; \sqrt{\frac{2}{3}} \cdot G \cdot \sqrt{E_1 \cdot E_2}\right)$
Hollow circular	AASHTO[18]	$\frac{2 \cdot t}{D} \cdot \frac{0.375 \cdot E_1}{\left(1 - \upsilon_{12}{}^2 \cdot E_2/E_1\right)^{0.5}}$ $\cdot 1.414 \cdot \left[\left(1 + \upsilon_{12} \cdot (E_2/E_1)^{0.5}\right) \cdot (E_2/E_1)^{0.5} \cdot (G/E_1)\right]^{0.5}$
Hollow circular	Campione[19]	$2 \cdot \frac{t}{D} \cdot \sqrt{\frac{E_1 \cdot E_2}{3 \cdot \left(1 - \upsilon_{12}{}^2\right)}} \cdot \sqrt{0.625 \cdot \left(\frac{E_2}{E_1}\right)^{0.85}}$

Table 4. Expressions for critical load

Author	Expression
Barbero and Tomblie[20]	$\left[\frac{1 + 1/\lambda_c^2}{1.30} - \sqrt{\left(\frac{1 + 1/\lambda_c^2}{1.30}\right)^2 - \frac{1}{0.65 \cdot \lambda_c^2}}\right] \cdot A \cdot F_{crl}$
Puente et al.[21]	$\frac{A \cdot F_{crl}}{0.5 \cdot \left[1 + 0.12 \cdot \left({\lambda_c}^2 - 0.25\right) + {\lambda_c}^2\right] + \sqrt{\left\{0.5 \cdot \left[1 + 0.12 \cdot \left({\lambda_c}^2 - 0.25\right) + {\lambda_c}^2\right]\right\}^2 - {\lambda^2}_c}}$
Cardoso et al.[14]	$\left(\frac{1 + \alpha + \lambda_c^2 \cdot \rho_p - \sqrt{\left(1 + \alpha + \lambda_c^2 \cdot \rho_p\right)^2 - 4 \cdot \lambda_c^2 \cdot \rho_p}}{2 \cdot \lambda_c^2}\right) \cdot A \cdot F_{crl}$
Strongwell Corporation[22]	$1.3 \cdot \frac{E_1 \cdot A}{(2 \cdot L/D)^{0.33}}$
ASCE[10]	$0.7 \cdot A \cdot \min\left(\frac{\pi^2 \cdot E \cdot J}{L^2 \cdot A}; \sigma_{cr}; \sigma_m\right)$

The same graph also shows the points related to the experimental investigations conducted by Yazhin and Ramesh,[23] Puente et al.,[21] and Yousis et al.[10] for hollow circular cross-sections. The case of square hollow cross-sections is not considered because it is not used here for members of bridge trusses. From the comparison in Fig. 7, the reduction of critical stress for local buckling is evident.

For the calculus of critical load of slender columns ASCE/SEI 74[10] adopts the expression of Eulero in the form

$$P_e = \frac{\pi^2 \cdot E \cdot J}{{l_0}^2} \tag{6}$$

where l_0 is the effective length of the element, and J the minimum moment of inertia. Using Eq. (6) and setting the critical stress equal to the compressive strength of the material (Eq. (5)) gives the limit slenderness of the elements equal to 17.

It is widely shown in the literature that for high slenderness values, the critical load predicted with the Eulero formula must be corrected, as done by Engesser,[24] to account for the shear contribution, as follows:

$$P_{Eg} = P_e \cdot \frac{1}{1 + k \cdot P_e/(G \cdot A)} \tag{7}$$

The values of k adopted in Eq. (7) are those suggested by Timoshenko and Gere[16] for isotropic materials, and for a thin-walled circular section and for a solid tube, they are equal to 0.5 and 0.75, respectively, and 5/6 for W shapes.

In the next sections, the critical load will be represented in the graphs against the mechanical λ_c or geometrical slenderness λ defined as:

$$\lambda_c = \sqrt{\frac{\min\left(\sigma_{cr}, \sigma_m\right) \cdot A}{P_e}} \quad \lambda = \frac{l_0}{(J/A)^{0.5}} \tag{8}$$

In pultruded members, because of the initial imperfections of elements, local and global interaction plays an important role in the values of the critical load, and several

authors propose analytical expressions for the calculation of the critical load taking into account the interaction between local and overall buckling, as shown in Table 4.

ASCE/SEI 74[10] considers the interaction between local and overall buckling and proposes calculating the critical load as

$$P_{cr} = \sigma_c \cdot A \cdot \frac{1 + 0.12 \cdot \left(\lambda^2 - 0.25\right) + \lambda^2 - \sqrt{1 + 0.12 \cdot \left[\left(\lambda^2 - 0.25\right) + \lambda^2\right]^2 - 4 \cdot \lambda^2}}{2 \cdot \lambda^2} \tag{9}$$

According to ASCE/SEI 74,[10] P_u is the minimum among $P_1 = \sigma_{cr} A$ (Table 4), P_e (Eq. 6), and P_{cr} (Eq. 9). In the equations shown in Table 4, F_{crl} is the minimum between the ultimate strength of the material in compression and the critical strength of the section.

Fig. 8 shows the variation of the ultimate stress (minimum between global buckling, local buckling, and compression material failure) as a function of the mechanical slenderness according to the different models considered. The theoretical values were calculated assuming $E_1 = 23$ GPa, $E_2/1/3\ E_1$, $G = 1/9\ E_1$, and $v = 0.23$. The same graph also reports the experimental data of Zhang et al.,[25] Zhang and Li[26]. From the comparison, it is clear that most of the models predict the experimental values with good approximation.

Numerical Example

In this section, we refer to pedestrian and road bridges of different spans L having truss structures as in Fig. 4 with elements featuring circular cross-sections of diameter 210 mm and thickness 15 mm. The deck is made of pultruded GFRP of height 400 mm with a span between the load-bearing trusses of 1.5 m. The deck has top and bottom flanges of 6 mm and webs of 6 mm at a pitch of 75 mm. The example refers to $E_1 = 30$ GPa ($E_2 = 1/3\ E_1$, $G = 1/9\ E_1$). The useful life chosen was 10 years.

The design load of the road bridge at the operating limit state was estimated at 9 kN/m^2 with a concentrated load of 30 kN in the middle of the beam. For pedestrian bridges a design load of 4 kN/m^2 was considered (half of the road bridge load and no concentrated load). In both cases (pedestrian and road bridges), the load on each beam is increased by 1.5 at the ultimate limit state and by 1.35 × ϕ, ϕ being the dynamic coefficient assumed in the Italian code as $\phi = 1 + 0.01 \cdot \frac{(100 - L)^2}{200 - L}$ according to CNR-DT 207.[8]

From a dynamic point of view, with reference to the scheme of a simply supported equivalent beam with mass M = P/g (where g is the gravitational acceleration) placed at the center of the beam, the vibration period of the first vibration mode is

$$T = 2 \cdot \pi \cdot \sqrt{P/g \left(\frac{L^3}{48 \cdot E_1 \cdot J} + \frac{\chi}{G \cdot A}\right)} \tag{10}$$

In Eq. (10), the viscoelastic effect and duration of the loads are taken into account for a period of 10 years with a 30% reduction of E1 and 50% of G, as suggested by CNR-DT 207.[8] According to the indications on the design of FRP

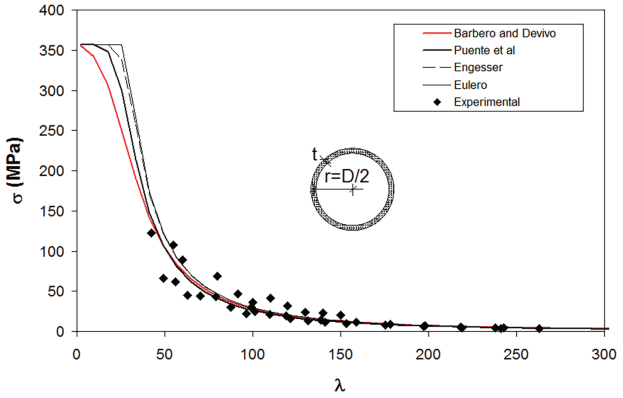

Figure 8. Global critical buckling stress versus mechanical slenderness

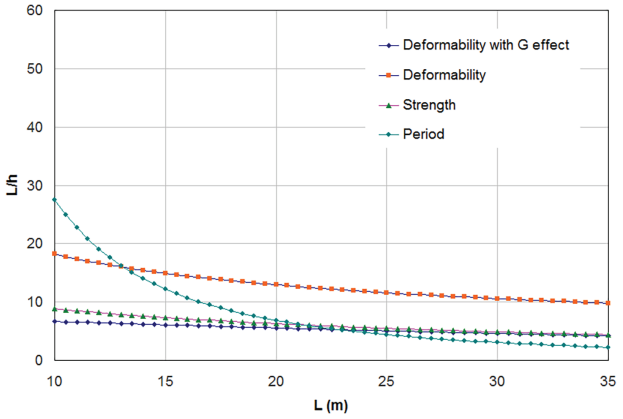

(a) Road bridge

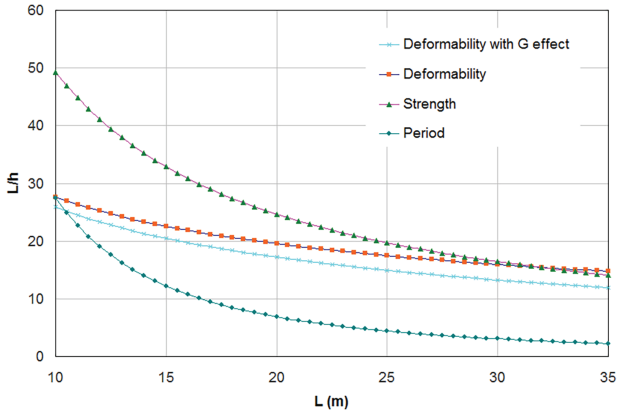

(b) Pedestrian bridge

Figure 9. Minimum ratios L/h with variation in L to respect limit states according to CNR-DT 207[8]

Bridges,[27] the fundamental frequency must be less than 5 Hz (period 0.2 sec) for vertical vibrations and 2.5 Hz (period 0.1 sec) for flexural and torsional vibrations. If the fundamental frequency is less than 3 Hz (0.33 sec) for horizontal or torsional vibrations, the use of dampers is recommended. If with Eq. (10) the limit of the period of 0.2 sec is imposed, it is possible to obtain the inertia of the beam.

Fig. 9 shows for case b) in Table 4 the variation in the ratio L/h with variation in L, for road and pedestrian bridges.

In the same graph, the minimum L/h ratios that satisfy the ultimate (strength) and serviceability limit states are shown. From the graph, it emerges that the design of GFRP bridges with D/t < 20 and $\lambda < 28$ is governed by deflection. By contrast, a check on the vibration period instead of the strength gives a limit of L/h = 15 for a pedestrian bridge and 5 for a road bridge. These are possible limits for a bridge of 35 m and 30 m and a footbridge of 10 m.

Conclusions

The specific application of GFRP truss structures could replace concrete deck and prestressed beams damaged by corrosion processes in single-span bridges while maintaining the piers and the foundation. This solution produces a significant reduction in seismic mass, with a consequent reduction of lateral forces on piers and foundation, and potentially cheaper strengthening of piers and foundation for seismic purposes. In this paper, a simple procedure for the design of temporary road bridges composed of GFRP truss beams and GFRP decks is shown. The model focuses on the choice of the best shape of truss structures and the geometry of the cross-section of the constituent elements, taking into account buckling effects and joint details to ensure the overstrength of the connections.

Major findings were that:

- Spatial truss structures having two upper chords or one chord having a circular cross-section with a diameter-to-thickness ratio lower than 54 is suggested, with a maximum geometrical slenderness of the upper chord of 17.
- The minimum height-to-span ratio of 1/5 and 1/15 of a span of 35 m are suggested to verify limit deflection of 1/500 of the span and a period lower than 0.2 sec for vertical vibration, also considering strength verification with long-term effects (10 years for a temporary bridge) and shear deformation contribution.
- Joints can be designed with bolted connections involving only steel plates at the joints and glued connections between steel elements and pultruded GFRP elements.

Data Availability

No data, models, or code were generated or used during the study.

References

[1] Azizinamini A. Full scale testing of old steel truss bridge. *J Constr Steel Res*. 2002;58(5–8):843–858. doi:10.1016/S0143-974X(01)00096-7.

[2] Yang X, Bai Y, Ding F. Structural performance of a large-scale space frame assembled using pultruded GFRP composites. *Compos Struct*. 2015;133(5):986–996. doi:10.1016/j.compstruct.2015.07.120.

[3] Zhu R, Li F, Shao F, Zhang D. Static and dynamic behavior of a hybrid PFRP-aluminum space truss girder: experimental and numerical study. *Compos Struct*. 2016;2020;243(14):112226. doi:10.1016/j.compstruct.2020.112226. [80]

[4] Khademi F, Zoruba S. In- and out-of-plane bending in steel through-truss bridges. *Pract Period Struct Design Constr*. 2023;27(2). doi:10.1061/(ASCE)SC.1943-5576.0000667.

[5] Higgoda TM, Elchalakani M, Kimiaei M, Wittek A, Yang B. Flexural behavior of pultruded circular tubular GFRP composite truss bridges with novel non-corrosive connections. *Structures*. 2022a;45:830–853. doi:10.1016/j10.1016/j.istruc.2022.09.063.

[6] Higgoda TM, Elchalakani M, Wittek A, Kimiaei M, Yang B. Investigation on the structural failure behaviour of pultruded circular tubular GFRP multiplanar truss bridges with non-metallic connections through finite element modeling. *Eng Fail Anal*. 2022b;142:106739. doi:10.1016/j.engfailanal.2022.106739.

[7] Higgoda TM, Elchalakani M, Kimiaei M, Yang B, Guo X. Experimental investigation on the structural behaviour of novel non-metallic pultruded circular tubular GFRP T-joints under axial compression. *Thin-Walled Struct*. 2023;184(12):110512. doi:10.1016/j.tws.2022.110512.

[8] CNR-DT 205/2007. Istruzioni per la Progettazione, l'Esecuzione ed il Controllo di Strutture realizzate con Profili Sottili Pultrusi di Materiale Composito Fibrorinforzato (FRP), Roma CNR. CNR-DT 205/2007; 2008. https://www.cnr.it/it/node/2625.

[9] CEN/TC 250 WG 4. Ascione, L. et al. FprEN/TS 19101: 2021 Design of Fiber-Polymer Composite Structures (November 2021) final version, duly referenced; 2021. https://eurocodes.jrc.ec.europa.eu/policies-standards/centc250-structural-eurocodes.

[10] ASCE/SEI 74. LRFD for Pultruded FRP Structures—A review of changes from the PreStandard, improvements, and needs for future editions; 2023.

[11] Bai Y, Yang X. Novel joint for assembly of all-composite space truss structures: conceptual design and preliminary study. *J Compos Constr*. 2013;17(1):130–138. doi:10.1061/(ASCE)CC.1943-5614.0000304.

[12] Li YF, Meda HA, Chen W. The design and analysis of internally stiffened GFRP tubular decks-a sustainable solution. *MPDI Sustain*. 2018;10(12):4538. doi:10.3390/su10124538.

[13] Hao X, Zhu R, Li R, Li F. Effect of joint stiffness on flexural performance of a hybrid FRP-aluminum space truss structure. *J Struct Eng*. 2021;147(12):04021214. doi:10.1061/(ASCE)ST.1943-541X.0003199.

[14] Cardoso DCT, Harries KA, Batista E de M. Compressive strength equation for GFRP square tube columns. *Compos Part B: Eng*. 2014;59(4):1–11. doi:10.1016/j.compositesb.2013.10.057.

[15] Pecce M, Cosenza E. Local buckling curves for the design of FRP profiles. *Thin-Walled Struct*. 2000;37(3):207–222. doi:10.1016/s0263-8231(00)00023-9.

[16] Timoshenko SP, Gere JM. *Theory of Elastic Stability*. New York: McGraw-Hill; 1961.

[17] Groenier JS, Eriksson M, Kosmalski S. *A Guide to Fiber-Reinforced Polymer Trail Bridges*. USA: Department of Transportation Federal Highway admistration. https://www.fs.usda.gov/eng/pubs/pdfpubs/pdf06232824/pdf06232824dpi72.pdf

[18] AASHTO. Issues Second Edition of GFRP Composite Material Guidebook. https://aashtojournal.transportation.org/aashto-issues-second-edition-of-gfrp-composite-material-guidebook/
[19] Campione. Strength and stability of pultruded GFRP elements. *Results in Engineering*. June 2025;26:105158.
[20] Barbero E, Tomblin J. A phenomenological design equation for FRP columns with interaction between local and global buckling. *Thin-Walled Struct*. 1994;18(2):117–131. doi:10.1016/0263-8231(94)90013-2.
[21] Puente I, Insausti A, Azkune M. Buckling of GFRP columns: an empirical approach to design. *J Compos Constr ASCE*. 2006;10(6):529–537.
[22] Corporation Strongwell. Strongwell design maual, Commonwealth Ave., Bristol, VA 24201 USA. (276) 645-8000; 2013.
[23] Yazhini A, Ramesh BC. Behavior of circular glass fiber reinforced polymer tubes under axial compression. *Int J Sci Eng Appl*. 2015;4(3):110–116.
[24] Engesser F. Die Knickfestigkeit gerader St¨abe. *Centralblatt der Bauverwaltung*. 1891;11:483. [111] Haringx JA. On.
[25] Zhan Y, Wu G, Harries KA. Determination of critical load for global flexural buckling in concentrically loaded pultruded FRP structural struts. *Eng Struct*. 2018;158(2):1–12. doi:10.1016/j.engstruct.2017.12.008.
[26] Zhang H, Li F. A review of prediction methods for global buckling critical loads of pultruded FRP struts. *Compos Struct*. 2024;329:1177752. doi: 10.1016/j.compstruct.2023.117752.
[27] Highway Structures & Bridges design—CD 368. Design of fibre reinforced polymer bridges and highway structures, DB 90/05; 2005.